J. Colgan
Graduate Research Assistant.

H. Chin
Graduate Research Assistant.

K. Danai
Associate Professor.

Department of Mechanical Engineering,
University of Massachusetts,
Amherst, MA 01003

S. R. Hayashi
GE Corporate Research & Development,
Schenectady, NY 12301

On-Line Tool Breakage Detection in Turning: A Multi-Sensor Method

A multi-sensor tool breakage detection system is introduced that characterizes the state of measurements during normal (no-fault) condition and at tool breakage by the two columns of a multi-valued influence matrix (MVIM). In this system the measurements are monitored on-line and flagged upon the detection of abnormalities. Tool breakage detection is performed by matching this vector of flagged measurements against the two columns of MVIM, which are estimated during a training session so as to minimize the error in detection. The detection system is implemented in turning. Experimental results indicate that this system provides excellent detection when the full range of tool breakage effect on the measurements is included in training, and that its performance is less dependent upon the training set than a multilayer neural net.

1 Introduction

Fracture will be the dominant mode of failure for more than one quarter of all advanced tooling material by the year 1995 (Powell, 1986). Therefore, on-line detection of tool breakages will be crucial to the realization of fully automated machining. Such a tool breakage detection system must be able to detect failures rapidly to prevent damage to the workpiece, and must be reliable so as to eliminate unnecessary downtime due to "false alarms."

Several measurements have been reported as good indicators of tool breakage (Tlusty and Andrews, 1983). Among these, the cutting force (Koenig et al., 1978), acoustic emission (Moriwaki, 1980; Lan and Dornfeld, 1984), spindle motor current (Matsushima et al., 1982), and machine tool vibration (Grieshaber et al., 1987) have been investigated extensively for their sensitivity to tool breakage. In general, to utilize a measurement for tool breakage detection, two requirements need to be satisfied. First, the measurement must reflect tool breakage under diverse cutting conditions (e.g., variable speeds, feeds, coolant on/off, workpiece material). Second, the effect of tool breakage on the measurement (tool breakage signature) must be uniquely distinguishable, so that other process irregularities such as hard spots and chip entanglement will not be confused with tool breakage. The effect of tool breakage on a measurement is commonly in the form of an abrupt change, in excess of a threshold value. Although considerable effort has been directed towards extracting reliable signatures of tool breakage from individual measurements (e.g., Lan and Naerheim, 1986; Altintas et al., 1988), no signature obtained from a single measurement has been so repeatable as to provide fool proof detection.

In order to extract more information from individual measurements so as to improve the reliability of tool breakage signatures, pattern classification techniques have been utilized. One of the earliest efforts was by Sata et al. (1973) who related features of the cutting force spectrum such as its total power, the power in the very low frequency range, and the power at the highest spectrum peak and its frequency to chip formation, chatter, and a built-up edge. It was shown that the cutting force measurement alone could provide sufficient information for unique identification of the above phenomena. Another important work in this category was performed by Kannatey-Asibu and Emel (1987) who applied a statistical pattern classification analysis to identify chip formation, tool breakage, and chip noise from acoustic emission measurements. They reported a success rate of 90 percent for tool breakage detection. Although the above studies have demonstrated that pattern classification is an effective method of enhancing the reliability of the tool breakage signature, the computational effort required to obtain the spectrum of the measurement precludes the application of these single-sensor based pattern classifiers for on-line tool breakage detection.

As an alternative to single-sensor based pattern classification, the integration of several sensors using artificial neural nets has been proposed for tool breakage detection (e.g., see Rangwala and Dornfeld, 1990; Tansel and McLaughlin, 1991). Artificial neural nets have the ability to represent fault signatures by complex decision regions without reliance on the probabilistic structure of the patterns. Thus, they are a powerful tool for fault detection/diagnosis. However, the ability of neural nets to form reliable fault signatures depends strongly upon their structure, as well as their training environment. In cases such as machining where adequate data is not available for net selection and comprehensive training, artificial neural nets may produce false alarms or leave faults undetected.

Contributed by the Production Engineering Division for publication in the JOURNAL OF ENGINEERING FOR INDUSTRY. Manuscript received Feb. 1992; revised Aug. 1992, Feb. 1993. Associate Technical Editor: E. Kannatey-Asibu, Jr.

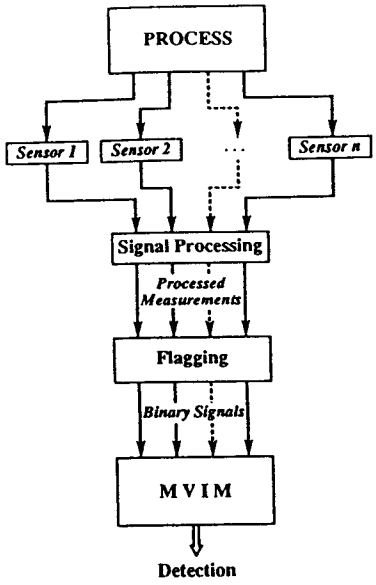

Fig. 1 Schematic diagram of the proposed sensor-based detection system

In this paper, a pattern classifying tool breakage detection system is introduced that has a fixed structure. Therefore, it does not require a selection phase, like artificial neural nets. Moreover, this method takes advantage of a fast learning algorithm that enables it to estimate the detection model based on a small number of training data. This system uses a *multi-valued influence matrix* (MVIM) as its detection model (Danai and Chin, 1991) that represents the *no-fault signature* and the *tool breakage signature* by its two columns, and performs detection by matching the two columns of the MVIM against a binary vector of flagged measurements that is produced by flagging the measurements. In this system, adaptation is performed at two levels. At one level, the columns of the MVIM are adjusted so that the error in detection is minimized. At the other level, flagging is tuned so as to produce binary flagged measurements suitable for detection.

The effectiveness of this tool breakage detection system is investigated in turning. Extensive tests were performed which produced six tool breakage cases. Four measurements: the ultrasonic energy, feed motor current, feed motor velocity, and machine vibration were measured and processed to enhance the effect of tool breakage. These measurements were then used as inputs to the MVIM and a multilayer neural net trained with backpropagation learning. Detection results indicate that the MVIM provided more robust detection than the multilayer neural net.

2 The MVIM Method

The MVIM method is based on a *multi-valued influence matrix* (MVIM) which represents the uncertain relationship between tool breakage and measurements (Danai and Chin, 1991). Measurements in this system are monitored in-process and converted to binary numbers through *flagging* (see Fig. 1). These flagged measurements are then posted in a vector of *flagged measurements* and matched against the individual columns of the influence matrix (influence vectors) for detection. In this system, influence vectors which represent the *no-fault signature* and the *tool breakage signature* are continuously updated by a learning algorithm to improve detection.

2.1 Detection Model. The multi-valued influence matrix A representing the *no-fault signature* and the *tool breakage signature* is defined as

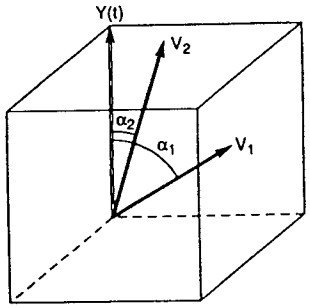

Fig. 2 Geometric representation of detection in the MVIM method

$$\mathbf{Y}(t) \overset{\mathbf{A}}{\Rightarrow} \mathbf{X}(t) \tag{1}$$

to relate the *flagged measurement vector* $\mathbf{Y}(t)$:

$$\mathbf{Y}(t) = [y_1(t), y_2(t), \ldots, y_m(t)]^T \tag{2}$$

to the fault vector $\mathbf{X}(t)$:

$$\mathbf{X}(t) = [x_1(t), x_2(t)]^T. \tag{3}$$

In the above equations, the vectors Y and X are binary vectors; i.e., the y_i (individual flagged measurements) and the no-fault variable x_1 and the fault variable x_2 can be equal to 0 or 1, representing the status of the particular measurement and fault at the time, respectively. The components of the $(m \times 2)$ influence matrix A have values between 0 and 1 defining the causal relationship between individual measurements and the fault and no-fault cases. For example, an $a_{12} = 0.8$ implies that the possibility of the first measurement being flagged at the instance of tool breakage is 0.8, or an $a_{31} = 0.2$ indicates that a 0.2 possibility exists that the third measurement is flagged during normal operation.

2.2 Detection. Detection in the MVIM method is based on measuring the closeness of individual influence vectors to the vector of flagged measurements. Closeness of vectors in the MVIM method is based on their orientation. Accordingly, the possibility of occurrence (*diagnostic certainty measure*) of the fault or no-fault variable is defined as the cosine of the angle between the corresponding influence vector and the vector of flagged measurements. The geometric representation of this reasoning is illustrated in Fig. 2, for a three dimensional measurement vector. Vectors V_1 and V_2 in this figure (the first and second columns of matrix A) represent the influence vectors associated with the no-fault and fault case, respectively, and vector Y is the vector of flagged measurements.

In the MVIM method, the vector of *diagnostic certainty measures* which ranks the variables x_1 and x_2 for their possibility of occurrence is defined as

$$\hat{X} = \begin{Bmatrix} \hat{x}_1 \\ \hat{x}_2 \end{Bmatrix} = \cos\{\alpha_j\} = \begin{Bmatrix} \cos\alpha_1 \\ \cos\alpha_2 \end{Bmatrix} \tag{4}$$

where the α_j (α_1 and α_2) denote the angles between the jth influence vector $\mathbf{V}_j$ ($\mathbf{V}_1$ and $\mathbf{V}_2$) and the flagged measurement vector Y. The angles α_j can be defined by their direction cosines to give

$$\hat{x}_j = \cos\alpha_j = \overline{\mathbf{V}}_j^T \overline{\mathbf{Y}}, \tag{5}$$

where $\overline{\mathbf{V}}_j$ and $\overline{\mathbf{Y}}$ are the normalized forms of vectors $\mathbf{V}_j$ and Y, respectively, defined as

$$\overline{\mathbf{V}}_j = \frac{\mathbf{V}_j}{\|\mathbf{V}_j\|} = \left\{ \frac{a_{ij}}{\sqrt{\Sigma_{i=1}^m a_{ij}^2}} \right\} \tag{6}$$

and

$$\overline{\mathbf{Y}} = \frac{\mathbf{Y}}{\|\mathbf{Y}\|} = \left\{ \frac{y_i}{\sqrt{\Sigma_{i=1}^m y_i^2}} \right\}. \tag{7}$$

Detection in the MVIM method is based on obtaining the vector of diagnostic certainty measures $\hat{\mathbf{X}}$. To obtain $\hat{\mathbf{X}}$, however, the normalized form of the influence matrix, $\bar{\mathbf{A}}$,

$$\bar{\mathbf{A}} = [\bar{\mathbf{V}}_1, \bar{\mathbf{V}}_2]$$

is required. Since this matrix is generally not known *a priori*, it will have to be estimated.

2.3 Estimation of $\bar{\mathbf{A}}$. One of the main features of the MVIM method is its capability to use the detection error as feedback in estimating/updating $\bar{\mathbf{A}}$. Based on this learning strategy, individual columns of the influence matrix are adjusted recursively when a flag is posted in a no-fault case, or after the occurrence of tool breakage, to minimize the sum of the squared detection error

$$J = \sum_{k_j=1}^{N_j} e_j(k_j)^2 = \sum_{k_j=1}^{N_j} [x_j(k_j) - \hat{x}_j(k_j)]^2 \tag{8}$$

The estimation algorithm of $\bar{\mathbf{A}}$, which is based on recursive least-squares estimation (Ljung, 1987), is given in (Danai and Chin, 1991), where its performance is demonstrated by simulation.

2.4 Flagging. In the MVIM detection system, flagging of measurements is performed by a Quantization Matrix. For flagging, the measurements are first scaled to produce a vector $\mathbf{Z} \in \Re^m$ with values between 0 and 1. Then they are multiplied by the weights of the Quantization Matrix, having the form

$$\mathbf{Q} = [\mathbf{W}_1, \ldots, \mathbf{W}_i, \ldots, \mathbf{W}_m], \tag{9}$$

and hard-limited as

$$y_i = \begin{cases} 1 & \text{when } \mathbf{Z}^T\mathbf{W}_i \geq 0.5 \\ 0 & \text{otherwise} \end{cases} \tag{10}$$

to produce the binary vector of flagged measurements $\mathbf{Y} \in \Re^m$ (defined in Eq. (2)). The vectors $\mathbf{W}_i$ in Eqs. (9) and (10) represent the columns of the Quantization Matrix associated with individual measurements.

The vectors of the MVIM are trained based on the flagged measurements y_i (see Eq. (10)). Therefore, they are directly influenced by the flagging operation. In order to improve the flagging operation, the Quantization Matrix is adapted in a training session. Ideally, we would like the magnitude of all the flagged measurements y_i to be equal to 0 for no-fault cases and 1 at tool breakages. To achieve this, the components of the Quantization Matrix are adjusted to produce an ideal flagged measurement vector of $[0\ 0\ 0\ 0]^T$ for no-fault cases, and a flagged measurement vector of $[1\ 1\ 1\ 1]^T$ at instances of tool breakage.

The Quantization Matrix uses a training set of measurement-fault vectors to tune its parameters iteratively. For this purpose, it uses recursive least-squares adaptation to minimize the sum of the squared errors between the individual flagged measurements produced by the Quantization Matrix and their ideal values. This learning algorithm has the form

$$w_{ij}(\mu) = w_{ij}(\mu - 1) + l_j(\mu - 1)[\tilde{y}_i(\mu) - \mathbf{Z}^T(\mu)\mathbf{W}_i(\mu - 1)] \tag{11}$$

where the w_{ij} denote the components of the Quantization Matrix, μ is the iteration step, $\tilde{y}_i$ represents the ideal value of flagged measurements (i.e., $\tilde{y}_i = 1$ for tool breakage cases, and $\tilde{y}_i = 0$ for no-fault cases), and the l_j denote the components of the adaptation gain vector $\mathbf{L} \in \Re^m$, which is updated according to the relationship (Ljung, 1987)

$$\mathbf{L}(\mu) = \frac{\mathbf{R}(\mu - 1)\mathbf{Z}^T(\mu)}{1 + \mathbf{Z}(\mu)\mathbf{R}(\mu - 1)\mathbf{Z}^T(\mu)}. \tag{12}$$

Matrix $\mathbf{R}$ denotes the covariance matrix in least-squares estimation, computed as

$$\mathbf{R}(\mu) = \mathbf{R}(\mu - 1) - \mathbf{L}(\mu)\mathbf{Z}(\mu)\mathbf{R}(\mu - 1) \tag{13}$$

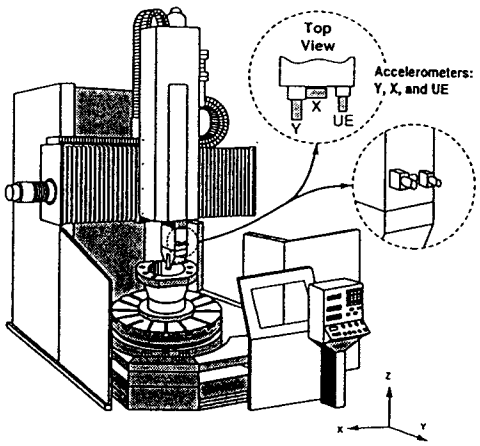

Fig. 3 Location of various sensors on the machine tool

Table 1 Parameters used in the experiments

Test #	Nominal Depth of Cut (mm)	Feed (mm/rev.)	Cutting Speed (m/sec.)
1	2.03	0.18	0.61
2	2.03	0.18	0.61
3	2.54	0.18	0.61
4	2.03	0.20	0.90
5	2.03	0.20	0.88
6	3.81	0.20	0.88

To implement the MVIM for detection, a training set is initially needed to tune the Quantization Matrix and estimate the MVIM. However, adaptation of MVIM does not necessarily need to be restricted to this initial training. Both the MVIM and Quantization Matrix, or the MVIM alone, can still be updated with each new tool breakage, or when a false alarm occurs, by taking advantage of the fast adaptation algorithm of MVIM.

3 Experimental

In order to test the feasibility of the MVIM method, turning experiments were performed at General Electric on a 37 kW NC vertical turret lathe (LVM125) with dc motor drives. The tools used were 35 degree diamond shaped tungsten carbide cam lock inserts and the tool holder used was a MVJNR 24-4 (side cutting edge angle = $-3°$, side rake angle = $-4°$ 15′, back rake angle = $-13°$ 20′). Two accelerometers (PCB 308B) were located on the ram of the lathe to measure the vibration in both the X and Y directions as illustrated in Fig. 3. Also located on the ram was a high frequency accelerometer (VM 1000), which was used to measure the ultrasonic energy (UE) of the cutting process in the 20 kHz to 80 kHz frequency range. A *Load Controls* power monitor was used to measure the spindle power, and the current inputs to the Z-carriage and X-carriage drive motors were measured using a simple shunt resistor. Signals proportional to the velocity components of the feed carriage in both the X and Z directions were obtained from the numerical control unit (GE MC 2000), and the spindle speed was measured by a once per revolution magnetic pickup. All sensory signals were recorded on a 14 track instrumentation tape recorder, and video images of the cutting tool and numerical control screen were also recorded together with a special time code signal to synchronize the video record with sensory signals.

Cutting tests consisted of straight internal cuts on Inconnel 718 cylindrical workpieces of approximately 48 cm inside diameter with the conditions listed in Table 1. Extensive testing was performed, of which six tests ending with tool breakage were analyzed. All breakage cases resulted in the loss of more than a third of the insert, usually in the middle of the lock pin area. As indicated in Table 1, in Tests #1, #2, #4, and #5 the

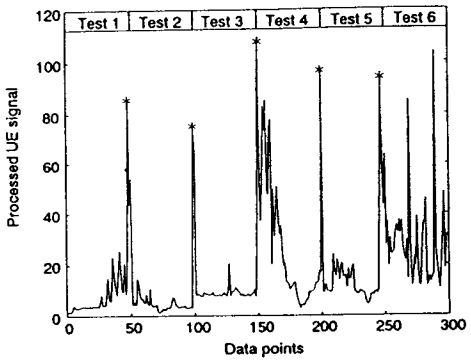

Fig. 4 Selected processed UE data for the six tests. Tool breakages are indicated by the asterisks.

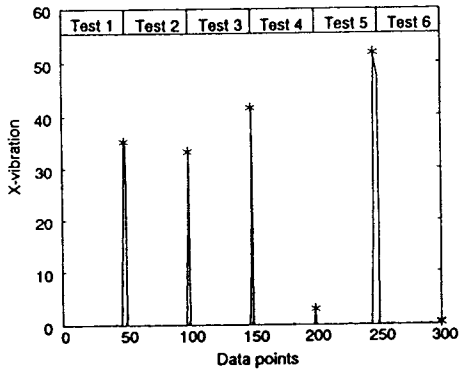

Fig. 5 Selected low frequency vibrations in the X direction for the six tests. Tool breakages are indicated by the asterisks.

cutting variables were constant, whereas in Tests #3 and #6 the depth of cut was gradually increased until tool breakage occurred. In all the tests cyclical variations in the depth of cut occurred due to workpiece out-of-roundness.

4 Signal Processing

In order to investigate the effect of tool breakage on various measurements, the exact time of each tool breakage was determined through video tapes. Thirty second windows around these times were then established for digitization purposes. Measurements in these time windows were low-pass filtered at 666 Hz and digitized at a sampling frequency of 2000 Hz. A preliminary examination of the digitized signals revealed a lag of as much as 0.0105 seconds in the effect of tool breakage on motor currents, which was associated with the response of the machine controller to the change in cutting load caused by tool breakage. In order to resolve this lag differential, so as to have the effect of tool breakage simultaneously reflected by all measurements, the data points contained in each 0.0125 second time interval (25 data points) were block averaged. As a result of block averaging, which is equivalent to applying a moving average filter to the data and then decimation, the data was reduced to a more manageable size, in effect reducing the sampling frequency to 40 Hz and aliasing the signal. Aliasing was not of major concern here because a frequency domain analysis was not used. In the following, the signal processing applied to each sensory signal to enhance the effect of tool breakage is discussed separately. Among the sensory signals, the spindle power was not used due to its insensitivity to tool breakage.

4.1 Ultrasonic Energy. The ultrasonic energy (UE) shares the same emission sources as acoustic emission (i.e., deformation in the shear zone, deformation and sliding friction at the tool-chip interface and tool-workpiece interface, and the breaking of chips and their impact on the cutting tool or workpiece), but covers a lower frequency range which allows placement of the transducer further away from the cutting zone (Hayashi et al., 1988). The UE signal was measured over a wide band (5 Hz to 80 kHz). This signal was then amplified, band pass filtered between 20 kHz and 80 kHz, full wave rectified, and RC averaged (the envelope of this processed signal was extracted) to enhance the effect of tool breakage (Hayashi et al., 1988). Figure 4 shows the processed UE signal for the selected time windows of the six tests. The results indicate that the processed UE signal reflects tool breakages (indicated by the asterisks), but also contains other spikes (particularly in Tests #4 and #6) that can be mistaken for the effect of tool breakage. If used by itself the processed UE signal would produce many "false alarms" depending on the threshold level. If the threshold is set higher the number of false alarms is reduced but tool breakage may be missed (e.g., in Test #6).

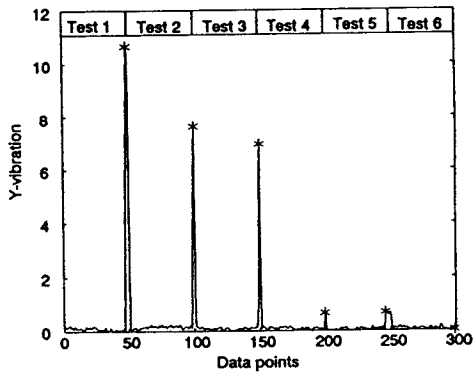

Fig. 6 Selected low frequency vibrations in the Y direction for the six tests. Tool breakages are indicated by the asterisks.

4.2 Low Frequency Vibration. Lower frequency vibrations (below 500 Hz) should be sensitive to loading changes of the tool carriage caused by tool breakage. The vibration signals originally measured in the frequency range of 0 to 666 Hz in the X and Y directions (see Fig. 3) on the ram of the feed carriage are shown in Figs. 5 and 6, respectively, for the selected time windows of the six tests. Both of these signals provide clear indication of tool breakage (indicated by the asterisks) except in Test #6. Thus, tool breakage detection based on either of these signals alone would result in at least one "undetected fault."

4.3 X and Z Feed Motor Currents and Velocities. Typical values of the feed motor currents and velocities in the X and Z directions are shown in Figs. 7–10. The results indicate that the current and velocity in the Z direction (feed direction) show a much more pronounced effect due to tool breakage (see Figs. 8 and 10), as compared to the current and velocity in the X direction (see Figs. 7 and 9). Note that the variation in the X-current and X-velocity are caused by workpiece out-of-roundness, and that the effective reflection of tool breakage by the Z-current and Z-velocity signals is perhaps enhanced by the severe cutting conditions used in the experiments. These signals may not provide such a consistent indication of tool breakage under less severe cutting conditions.

A common method of examining abnormalities in a signal is through modeling the signal during normal operation, so that any mismatch between the signal and its modelled value can be detected through the residual (Isermann, 1984). Since tool breakage is expected to affect the load of the drive system, an ARX model (Ljung, 1987) of the drive system in the Z

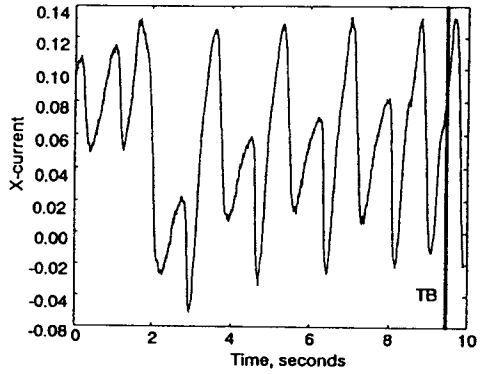

Fig. 7 Typical values of the feed motor current in the X direction. The vertical line TB indicates tool breakage.

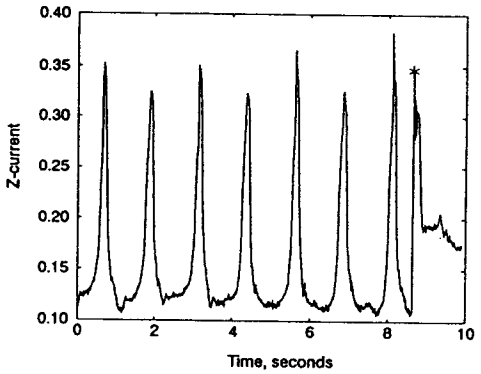

Fig. 8 Typical values of the feed motor current in the Z direction. Tool breakage is indicated by the asterisk.

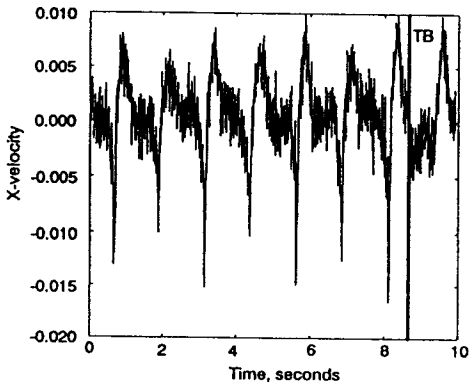

Fig. 9 Typical values of the feed motor velocity in the X direction. The vertical line TB indicates tool breakage.

direction was developed with the Z-current as the input and Z-velocity as the output. One drawback with this model is that it would only represent the dynamics of the feed drive system under nominal friction and cutting loads. Therefore, any cutting load changes due to different cutting variables, hard spots, chip entanglement, or changes in the frictional behavior of the machine ways will be reflected in the residual as noise. While such noise may be significant for machining parts with complex geometry or interrupted cutting, the cutting load changes in the present experiments were insignificant since the cutting variables were essentially constant in the six tests. Also frictional changes were expected to be small since the machine ways utilized recirculating roller pack bearings.

For modeling purposes, the data from Test #3 was utilized

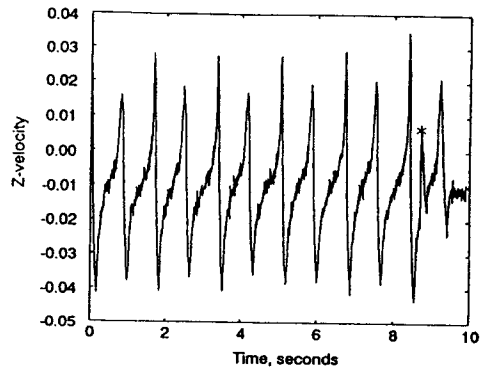

Fig. 10 Typical values of feed motor velocity in the Z direction. Tool breakage is indicated by the asterisk.

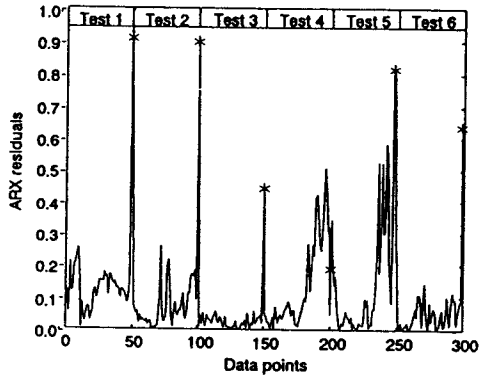

Fig. 11 Selected residuals of the ARX model for the six tests. Tool breakage is indicated by the asterisks.

to develop a fourth order ARX model with one delay based on a 95 percent confidence interval for both the autocorrelation of the residuals and the cross-correlation between the residuals and the inputs (Ljung, 1987). Figure 11 shows the sensitivity of the residuals obtained by subtracting the output of the ARX model from the actual value of the Z-velocity for the time windows of the six tests. The residuals detect tool breakages (indicated by the asterisks) but, like the processed UE signal, contain many spikes (particularly in Tests #4 and #5) that cannot be distinguished from the effect of tool breakage.

5 Detection Results

As noted in the previous section, none of the four measurements: (*1*) the processed UE signal, (*2*) X-vibration, (*3*) Y-vibration, and (*4*) residuals of the ARX model between the Z-current and Z-velocity reliably identify tool breakage. As such, they provide a suitable basis for testing the effectiveness of MVIM in multi-sensor detection. Note that the measurements used and the associated signal processing are specific to the present study, and are not proposed as suitable in a generic sense. For example, had the cutting conditions been variable during the experiments (e.g., variable feedrates or depth of cut) the signal processing would have been performed such that the resulting measurement changes would be accounted for (Koren et al., 1991).

For training and testing purposes, the data points from the time windows of the six turning tests were used to represent the normal behavior of the measurements as well as their reflection of tool breakages (see Figs. 4, 5, 6, and 11). However, before the measurements were used for training and testing the MVIM, their linear separability for the normal and tool breakage categories were checked. Linearly separable categories can be readily identified on the two sides of a plane between hard-limited measurements, and do not require advanced pattern classification. To check linear separability, a

Table 2 Detection results obtained by MVIM and a multi-layer neural net trained with different data sets

Case #	Training Data Sets	Detection Method	Undetected Faults	False Alarms
1	3, 5	MVIM	1	0
		Neural Net	0	12
2	3, 4	MVIM	1	0
		Neural Net	0	0
3	4, 5	MVIM	1	0
		Neural Net	1	0
4	5, 6	MVIM	0	0
		Neural Net	1	0
5	2, 5, 6	MVIM	0	0
		Nerual Net	1	0
6	2, 4, 5	MVIM	1	0
		Neural Net	1	0
7	2, 3, 5	MVIM	1	0
		Neural Net	0	12
8	2, 3, 6	MVIM	0	1
		Neural Net	0	0
9	1, 2, 3, 4	MVIM	1	0
		Neural Net	0	0
10	1, 2, 3, 6	MVIM	0	1
		Neural Net	0	0
11	1, 2, 5, 6	MVIM	0	0
		Neural Net	1	0
12	1, 2, 4, 6	MVIM	0	0
		Neural Net	2	0

single-layer perceptron using least mean square (LMS) adaptation (Lippmann, 1987) was trained on the measurements from the six tests until the mean square error was stabilized. This perceptron was then used to detect the tool breakages in the tests. The perceptron produced several false alarms, indicating that the two categories were not linearly separable.

The relative effectiveness of MVIM was then evaluated by comparison with a multilayer neural net trained with the back-propagation learning algorithm (Rumelhart et al., 1988). The comparison made here was of course a limited one, involving only one type of neural net. However, this comparison was included so as to highlight the characteristic differences between the MVIM and neural nets insofar as the requirements for their implementation. In order to investigate the robustness of detection with respect to the training set, the measurements from the six tests were grouped into different combinations for training as indicated in Table 2. Testing, however, was performed based on data from all of the tests. For each training case in Table 2, the initial values of the influence matrix $\mathbf{A}$, and Quantization Matrix $\mathbf{Q}$ were set to zero and identity, respectively, and the initial covariance matrix $\mathbf{R}$ in Eq. (13) was set to identity. Unlike the MVIM which has a fixed structure, the topology of neural nets needs to be selected based on their generalization ability pertaining to correct classification of patterns not included in training (Hertz et al., 1991). Therefore, neural nets with different number of hidden units, learning rate, and momentum coefficient were trained with the training sets in Table 2 and tested with all of the test sets. For training purposes, two outputs were considered for the net with their target values set at $[1\ 0]^T$ and $[0\ 1]^T$ for the no-fault case and the fault case, respectively. In all cases, the nets were trained with the same measurements used in training the Quantization Matrix. Based on extensive trial and error involving a wide range of parameters, the neural net which provided the best overall results had 4 hidden units, the learning rate of 0.5, and the momentum coefficient of 0.8 (Rumelhart et al., 1988). Note that because of its fixed structure, the MVIM did not require trial and error testing.

For both the MVIM and neural net, after each epoch (pass through the training set) the detection performance of the system was evaluated within the training set. Detection by MVIM consisted of first flagging each vector of measurements by the Quantization Matrix and then analyzing the flagged measurement vector through the MVIM. In all cases, in order to avoid overtraining, training for both the MVIM and neural net was stopped once all the tool breakages were detected and no false alarms were generated within the training set. Note that training could be continued until a zero vector was obtained for the first column of MVIM (the no-fault signature). However, experience shows that such a training procedure results in overtraining the MVIM and its poor generalization performance. A typical MVIM obtained for Case #3 is shown below,

$$\hat{\mathbf{A}} = \begin{bmatrix} 0.09 & 0.43 \\ 0.15 & 0.52 \\ 0.91 & 0.52 \\ 0.39 & 0.52 \end{bmatrix} \tag{14}$$

which indicates that effective detection was achieved within the training set with a non-zero no-fault signature (i.e., the first column). In all cases the MVIM converged after one epoch, whereas the neural net required a few hundred epochs for most training cases.

The detection results obtained from the MVIM and the neural net trained with different training sets are shown in Table 2. The results indicate that the performance of both the MVIM and the neural net was dependent upon their training sets, and that they produced comparable results, except for the large number of false alarms produced by the neural net in Cases #1 and #7. Note that the MVIM produced at most one false alarm or undetected fault in each case, indicating a more robust performance.

6 Conclusions

Multi-sensor tool breakage detection is demonstrated based on the MVIM method. This method benefits from fast learning and a fixed structure, which makes it independent of a selection phase. Extensive experiments were performed, of which six tests ending with tool breakage were analyzed. Four measurements were obtained which reflected the effect of tool breakage. These measurements were utilized as inputs to the MVIM and a multi-layer neural net using back-propagation learning. Detection results indicate that the MVIM was less sensitive to its training environment than the neural net. The robustness of MVIM, coupled with its fixed structure and fast learning are important from the point of view of implementation. While the results of this study indicate the effectiveness of MVIM in sensor integration, more testing is required before the MVIM can be applied on the shop floor. A key element is a set of measurements and signal processing techniques that will provide adequate reflection of tool breakage under diverse cutting conditions.

Acknowledgments

The authors would like to express their gratitude to Dr. B. Keramati of GE for his support of this project. This work was supported in part by the National Science Foundation (Grant No. MSS-9102149).

References

Altintas, Y., Yellowley, I., and Tlusty, J., 1988, "The Detection of Tool Breakage in Milling Operations," ASME JOURNAL OF ENGINEERING FOR INDUSTRY, Vol. 110, No. 3, pp. 271-277.

Danai, K., and Chin, H., 1991, "Fault Diagnosis With Process Uncertainty," ASME *Journal of Dynamic Systems, Measurement, and Control*, Vol. 113, No. 3, pp. 339-343.

Grieshaber, D., Ramalingam, R., and Frohrib, D., 1987, "On Real-Time Tool Fracture in Milling," *Proc. of 15th NAMRC*, May, pp. 477-484.

Hayashi, S. R., Thomas, C. E., and Wildes, D. G., 1988, "Tool Break Detection By Monitoring Ultrasonic Vibrations," *Annals of the CIRP*, Vol. 37, No. 1, pp. 61–64.

Hertz, J., Krogh, A., and Palmer, R. G., 1991, *Introduction to the Theory of Neural Computation*, Addison Wesley, Reading, MA.

Isermann, R., 1984, "Process Fault Detection Based on Modeling and Estimation Methods—A Survey," *Automatica*, Vol. 20, No. 4, pp. 387–404.

Kannatey-Asibu, E., and Emel, E., 1987, "Linear Discriminant Function Analysis of Acoustic Emission Signals for Cutting Tool Monitoring," *Mechanical Systems and Signal Processing*, Vol. 4, pp. 333–347.

Koenig, W., Kluft, W., and Froehlich, R., 1978, "Automatische Werkzeugbrucherkennung bei der Drehbearbeitung (Automated Detection of Tool-Breakage in Turning," *Industrie-Anzeiger*, Vol. 100, No. 28, pp. 62–63.

Koren, Y., Ko. T., Ulsoy, A. G., and Danai, K., 1991, "Flank Wear Estimation Under Varying Cutting Conditions," ASME *Journal of Dynamic Systems, Measurement, and Control*, Vol. 113, No. 2, pp. 300–307.

Lan, M., and Naerheim, Y., 1986, "In-Process Detection of Tool Breakage in Milling," ASME JOURNAL OF ENGINEERING FOR INDUSTRY, Vol. 108, August, pp. 191–197.

Lan, M. S., and Dornfeld, D. A., 1984, "In-Process Tool Fracture Detection," ASME *Journal of Engineering Materials and Technology*, Vol. 106, April, pp. 111–118.

Lippmann, R. P., 1987, "An Introduction to Computing with Neural Nets," *IEEE ASSP Magazine*, pp. 4–22.

Ljung, L., 1987, *System Identification—Theory for the User*, Prentice-Hall, Englewood Cliffs, NJ.

Matsushima, K., Bertok, P., and Sata, T., 1982, "In-Process Detection of Tool Breakage by Monitoring the Spindle Motor Current of a Machine Tool," *Measurement and Control for Batch Manufacturing*, ASME, pp. 145–154.

Moriwaki, T., 1980, "Detection for Tool Fracture by Acoustic Emission Measurement," *Annals of the CIRP*, Vol. 29, No. 1, pp. 35–40.

Powell, J. W., 1986, "In Process Control for Manufacturing," *IEEE 15th Video Conference*, Vol. 2, Sept.

Rangwala, S., and Dornfeld, D., 1990, "Sensor Integration Using Neural Networks for Intelligent Tool Condition Monitoring," ASME JOURNAL OF ENGINEERING FOR INDUSTRY, Vol. 112, pp. 219–228.

Rumelhart, D. E., Hinton, G. E., and Williams, R. J., 1988, "Learning Error Representation by Error Propagation," Rumelhart, D. E., and McClelland, J. L., eds., *Parallel Distributed Processing—Explorations in the Microstructure of Cognition*, MIT Press, Cambridge, MA.

Sata, T., Matsushima, K., Nagakura, T., and Kono, E., 1973, "Learning and Recognition of the Cutting States by the Spectrum Analysis," *Annals of the CIRP*, Vol. 22, pp. 41–42.

Tansel, I. N., and McLaughlin, C., 1991, "On-Line Monitoring of Tool Breakage with Unsupervised Neural Networks," *Trans. of NAMRC*, SME, pp. 364–370.

Tlusty, J., and Andrews, G. C., 1983, "A Critical Review of Sensors for Unmanned Machining," *Annals of the CIRP*, Vol. 32, No. 2, pp. 563–572.